ELSEVIER

Surface Science 491 (2001) 140–148

SURFACE SCIENCE

www.elsevier.com/locate/susc

Step-modified phase diagram of chemisorbed oxygen on nickel

T.P. Pearl [1], S.B. Darling, S.J. Sibener *

Department of Chemistry, The James Franck Institute, The University of Chicago, 5640 South Ellis Avenue, Chicago, IL 60637, USA

Received 10 April 2001; accepted for publication 22 June 2001

Abstract

We have studied the effect of an extended array of steps on the two-dimensional phase behavior of chemisorbed oxygen overlayers on a vicinal nickel surface using low energy electron diffraction (LEED), Auger electron spectroscopy, and scanning tunneling microscopy. Phase behavior of oxygen on the vicinal Ni(9 7 7) surface was examined and compared with that for oxygen adsorbed on the flat Ni(1 1 1) surface. There are two significant differences in the phase diagrams for these two surfaces. On Ni(1 1 1) at $\theta = 0.25$ ML, oxygen forms a $p(2 \times 2)$ structure that disorders to a lattice gas at 440 K and remains disordered until it is ultimately dissolved into the bulk above 500 K. Surface defects, such as the steps on Ni(9 7 7), substantially modify this phase progression. On Ni(9 7 7), the $p(2 \times 2)$ phase still disorders at 440 K, but a second ordered phase, which can be designated as Ni[8(1 1 1) × (1 0 0)]–2(1d)-O in microfacet notation, exists between room temperature and above 500 K when the oxygen is finally incorporated into the bulk. This adsorbate phase is step-stabilized and can be generated by dosing the surface with a small amount of oxygen or as a result of partial dissolution of oxygen from the higher coverage $p(2 \times 2)$ phase. Moreover, anisotropic disordering effects are evident due to the presence of the steps as indicated by the increasingly oblate shape of diffraction spots as the $p(2 \times 2)$ disorders. The process of oxygen dissolution is also qualitatively altered by the presence of regular steps.

Keywords: Oxygen; Nickel; Chemisorption; Low energy electron diffraction (LEED); Stepped single crystal surfaces; Surface structure, morphology, roughness, and topography; Vicinal single crystal surfaces; Oxidation

1. Introduction

The interaction of oxygen with metal surfaces is of great interest in areas such as corrosion, catalysis, and fundamental studies of two-dimensional phase transitions. Nickel, in particular, has been the focus of many studies on oxidation [1–13], phonon dispersion [14], surface reconstruction [15–19], and critical phenomena [20,21]. However, the degree to which local morphological features, specifically deviations from perfect crystalline planes, influence surface processes and reaction pathways has only recently been assessed directly using probe microscopies. Defects like steps have been shown to act as reactive centers [22], trapping and aggregating adspecies with their higher coordination sites [23], and to exhibit modified electronic potential [24,25] and localized surface phonon structure [26]. In this study we examine

* Corresponding author. Tel.: +1-773-7027193; fax: +1-773-7025863.

E-mail address: s-sibener@uchicago.edu (S.J. Sibener).

[1] Present Address: Department of Chemistry, The Pennsylvania State University, 152 Davey Laboratory, University Park, PA 16802, USA.

0039-6028/01/$ - see front matter
PII: S0039-6028(01)01388-7

the interaction of oxygen with Ni(9 7 7) using low energy electron diffraction (LEED), supplemented with Auger electron spectroscopy (AES) and scanning tunneling microscopy (STM). The stepped surface studied in this experiment consists of eight atom wide (1 1 1) terraces separated by monatomic (1 0 0) steps (Fig. 1). Differences between the behavior of this system and O/Ni(1 1 1) can therefore be attributed to step effects and finite terrace sizes. Our findings suggest a step-induced deviation in oxygen behavior with ramifications extending to the rate of bulk metallic oxidation.

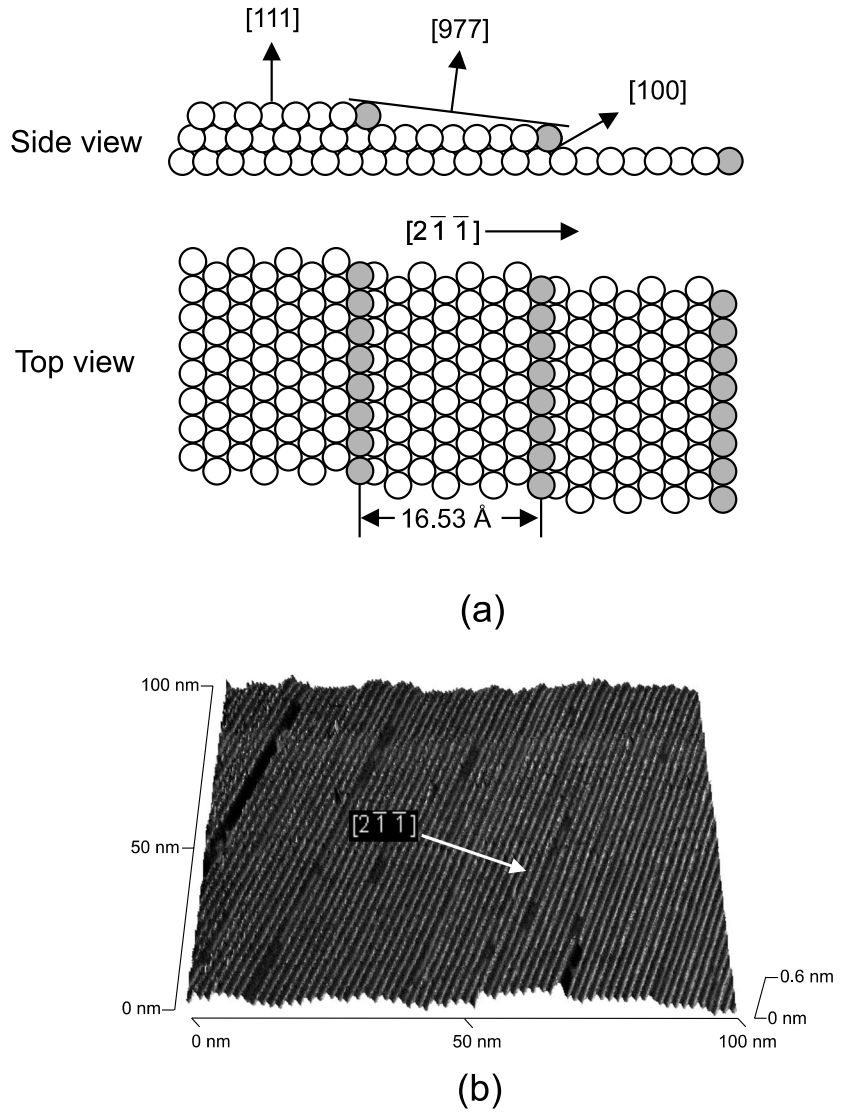

Fig. 1. (a) A schematic of the Ni(9 7 7) surface as viewed from the side and from above. The surface consists of (1 1 1) terraces which are eight atoms wide and separated by single atom high steps. Several high symmetry directions are indicated. (b) STM image of clean Ni(9 7 7) at 298 K recorded with a tunneling current of 1 nA and 100 mV positive sample bias with respect to the tip.

2. Experimental

These experiments were carried out in a two-level ultra-high vacuum (UHV) chamber pumped with a 220 L/s D–I ion pump, cryoshroud and titanium sublimation pumps, as well as a 55 L/s turbo-molecular drag pump used for pumping sputtering gases and chamber bakeouts. A base pressure of 5.5×10^{-11} Torr is routinely achieved after a standard bakeout cycle. The chamber is equipped with retractable, reverse view, four-grid LEED optics for surface diffraction that are also used as a retarding field analyzer for AES. The lower-level houses a variable temperature STM with an operational range of room temperature to 650 K attained via radiative heating from a filament located behind the crystal [27]. Sputtering and reagent gases were dosed by chamber back-filling using high precision leak valves. Oxygen was dosed by back-filling the chamber with O_2 to a pressure of 1×10^{-9} Torr. The Ni(9 7 7) crystal used in these studies was cleaned by repeated cycles of sputtering with 1 keV Ar^+ ions followed by annealing above 1000 K by electron bombardment of the rear of the crystal until carbon and sulfur levels were below our Auger detection limit. A sharp LEED pattern with well defined splitting of the (1 1 1) terrace spots (characteristic of the stepped surface) at all temperatures confirmed surface crystallinity. STM data of this surface demonstrate a low kink density and narrow terrace width distribution (Fig. 1).

LEED patterns at $E_i = 25.6$ eV were recorded to measure the disordering behavior for O/Ni(9 7 7) with surface temperatures ranging from 298 to 565 K. The surface was heated radiatively by a tungsten filament located behind the crystal and dwelled at each temperature for ~5 min. LEED patterns at each temperature were photographed with constant power delivered to the filament to avoid fluctuating field effects on diffraction spot intensities and widths [28]. Photographs were digitized to facilitate analysis of spot profiles. Several factors affected the analysis of these profiles. As the temperature was increased, a background luminescence from the crystal heating element progressively inhibited spot detection on the phosphorus screen. Another effect of increasing temperature was progressive dissolution of oxygen into the bulk, effectively reducing the strength of the oxygen LEED pattern. The openness of the O/Ni system, i.e., the capability of oxygen to leave the surface through dissolution, complicates dissection of the phase diagram. This dissolution process was tracked with AES (Fig. 3a) and a corrective deconvolution was applied in the analysis of the data. For the purposes of deconvoluting data, oxygen dissolution was treated as an isotropic process, but oxygen remains near the step edges at higher temperatures than on the terraces. The dissolution behavior for oxygen on this surface as it relates to the LEED data will be discussed later.

3. Results

3.1. Oxygen overlayer geometry: LEED and STM

In the limit of low coverage, less than 2% of a monolayer, oxygen atoms adsorb to the bottom of the Ni(9 7 7) step edges due to the favorable four-fold coordination available from the (1 0 0) step faces. Studies on other vicinals with (1 0 0) step geometry have confirmed this location for adsorbed oxygen in the limit of low coverage [29–31]. For adsorption at room temperature in this low coverage limit, the oxygen adsorbed at the steps forms a previously unobserved ordered $(n \times 2)$ structure exhibiting weak diffraction. With further exposure at room temperature, oxygen forms an ordered $p(2 \times 2)$ superstructure at a coverage of 0.25 monolayers (1 ML $\equiv$ 1 oxygen per Ni(1 1 1) surface unit cell). As the substrate is heated, this phase undergoes an order–disorder transition at 438–440 K both for the flat Ni(1 1 1) [20,21,32,33] and stepped Ni(9 7 7) (Figs. 2 and 3b). However, the step-localized $(n \times 2)$ phase, also seen at lower coverage, begins to appear together with the $p(2 \times 2)$ around room temperature and persists well above the $p(2 \times 2)$ disordering transition temperature. There are, therefore, two routes to form the $(n \times 2)$ phase: directly, using a low exposure of oxygen, or indirectly, by dissolution from $\theta =$ 0.25 ML; the latter approach results in superior diffraction, presumably due to kinetic effects. The

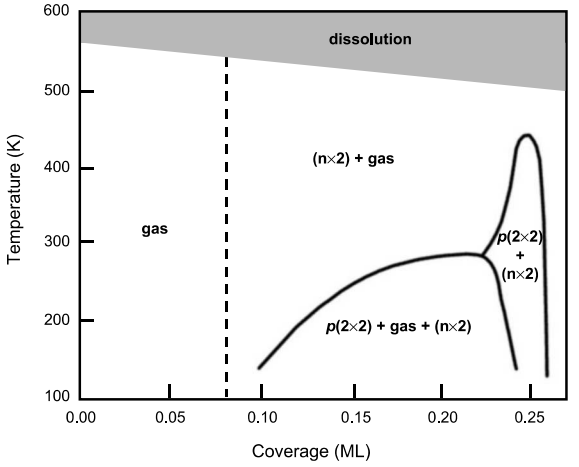

Fig. 2. Schematic phase diagram for oxygen on Ni(9 7 7). The step-stabilized $(n \times 2)$ oxygen structure coexists with other ordered and disordered phases of oxygen over a wide range of both temperature and coverage. The dotted line at $\theta = 0.08$ ML represents a half-titration of the step edges; this is the optimal coverage for the $(n \times 2)$ phase. Phase boundaries involving the $p(2 \times 2)$ phase are adapted from Ref. [21] and those involving the $(n \times 2)$ phase are qualitative assignments from our experiment. The gray dissolution region qualitatively summarizes more complicated absorption behavior. For details regarding higher coverage phases, see Fig. 1 in Ref. [21].

step-stabilized ordered overlayer remains locked in place until it is finally incorporated into the bulk around 565 K. This dissolution temperature is dependent on the oxygen dissolution history of a particular crystal. Lower temperatures for oxygen incorporation into nickel have been reported for crystals with less oxidation history [32,34]. A plot of the diffraction intensities for the $(\frac{1}{2}, \frac{1}{2})$ and a representative spot from the $(n \times 2)$ structure as a function of substrate temperature, corrected for oxygen dissolution and Debye–Waller attenuation, is presented in Fig. 3b. The Debye temperature (160 K) was assumed to be the same as that of O/Ni(1 1 1) [21]. While our data were too noisy to extract a critical exponent for the $p(2 \times 2) \rightarrow$ lattice gas transition, Sokolowski and Pfnür's work on ruthenium surfaces [35] and work in our group with H/Ni(9 7 7) [36] suggests that reduced symmetry resulting from the introduction of a regular array of steps should convert this system from the expected 4-state Potts universality class to a two-dimensional Ising-like transition. As shown in

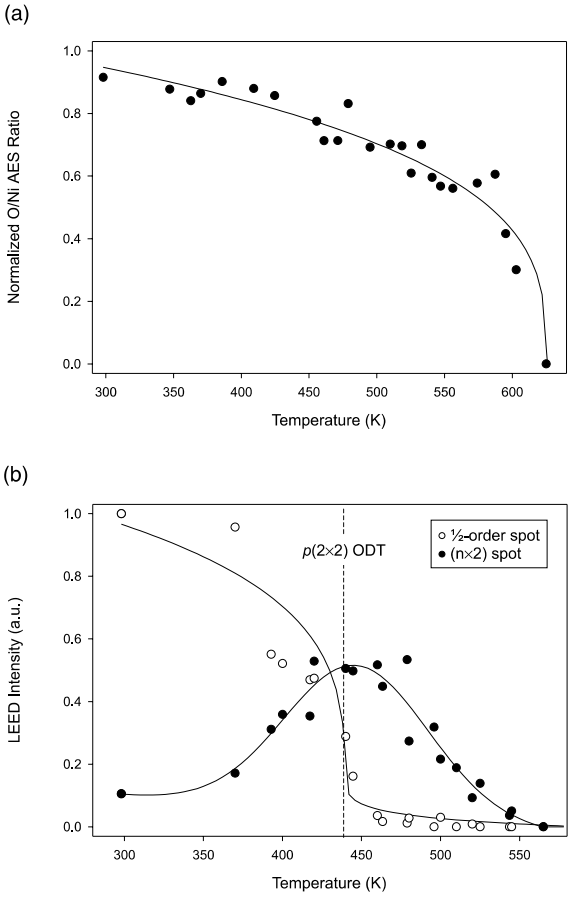

Fig. 3. (a) Oxygen (510 eV)/Nickel (848 eV) AES peak ratio as a function of sample temperature normalized to $\theta = 0.25$ ML coverage. The line through the data serves only to guide the eye. The falloff is due to oxygen incorporation into the bulk. (b) LEED intensity as a function of substrate temperature corrected for oxygen dissolution and Debye–Waller attenuation for both the $p(2 \times 2)$ and $(n \times 2)$ phases. The oxygen dose was 0.56 Langmuirs at room temperature. The lines through the data serve only to guide the eye. Maximal order for the $(n \times 2)$ phase coincides approximately with the $p(2 \times 2)$ disordering inflection point. The intensities are only applicable in the case of increasing temperature because of irreversible oxygen dissolution into the bulk.

Fig. 3b, the diffraction signature for the $(n \times 2)$ structure coexists, albeit weakly, with the $p(2 \times 2)$ between just above room temperature and 440 K, where the $p(2 \times 2)$ completely disorders. Note that the LEED intensities that are tracked in Fig. 3b only hold true if the sample temperature is increased due to irreversible dissolution. If the

sample is cooled to room temperature after reaching 565 K, where diffraction for the overlayer disappeared, the only visible spots are from the substrate terrace, indicating complete dissolution of surface oxygen into the bulk [12,20,32].

Using an intentionally-stepped substrate to secure an ordered superstructure is not a technique limited to this system. In a previous experiment [36], we observed a similar step-induced stabilization of an ordered overlayer with H/Ni(9 7 7). Also, Sokolowski and Pfnür reported a modest expansion of the ordered $p(2 \times 2)$-O region of the phase diagram on stepped Ru(0 0 0 1) [35].

Additional evidence for step edge influence is that the $p(2 \times 2)$ LEED spots appear increasingly oblate as the superstructure disorders. The longer axis is aligned along the $\langle 2\bar{1}\bar{1} \rangle$ azimuth corresponding to disordering preferentially occurring perpendicularly to the step edges. Fig. 4 illustrates the difference in spot shape for the $p(2 \times 2)$ spots between room temperature and the order–disorder transition temperature. As the surface is heated, this aspect ratio becomes more pronounced. This diffraction anisotropy suggests that the $p(2 \times 2)$ domains disorder in the center of the terraces before disordering in the vicinity of the step edges.

Diffraction from the $(n \times 2)$ structure formed via dissolution from the higher coverage phase results in rows of spots in both the (1 1 1) and half-order planes (Fig. 5). Spot intensities were relatively weak compared to the $p(2 \times 2)$ and all of the resolvable spots for this new structure could only be realized after the sample was cooled to room temperature to minimize Debye–Waller attenuation. This oxygen structure formed on Ni(9 7 7) can be designated as Ni[8(1 1 1) × (1 0 0)]–2(1d)-O in microfacet notation. This structure, where oxygen occupies every other step edge trough site, is schematically drawn in Fig. 6. Its diffraction signature is most similar to that seen by Lang et al. of oxygen on a stepped platinum surface where streaking was clearly evident along both (1 1 1) and half-order rows [30]. A similar result has also been reported for O/Ni(1 1 9) by Dorsett et al. [31]. They observed extra spots in between the terrace split spots, which they confirmed were due to an oxygen overlayer at the bottom of the step edges and not simply step edge diffraction.

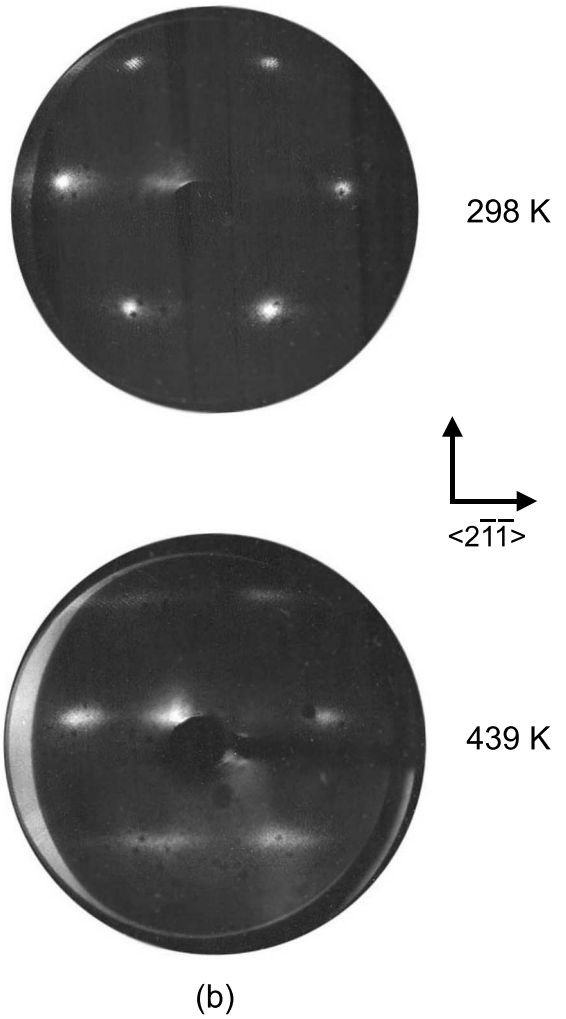

Fig. 4. LEED pattern ($E_i = 25.6$ eV) of $p(2 \times 2)$-O at 298 K and at 439 K. Note the oblate shape of the spots at the order–disorder transition temperature. The long axis of these spots is aligned along the $\langle 2\bar{1}\bar{1} \rangle$ azimuth implying anisotropic disordering, with the oxygen disordering in the center of the terraces before doing so in the vicinity of the steps.

In addition to capturing the temperature dependent behavior of the two ordered structures by photography, much effort was made by visual inspection to determine the registry of the structures to the underlying substrate. By choosing to view the electron diffraction at two specular conditions, with either the terrace or the step plane normal to the electron gun, we could track the motions of the

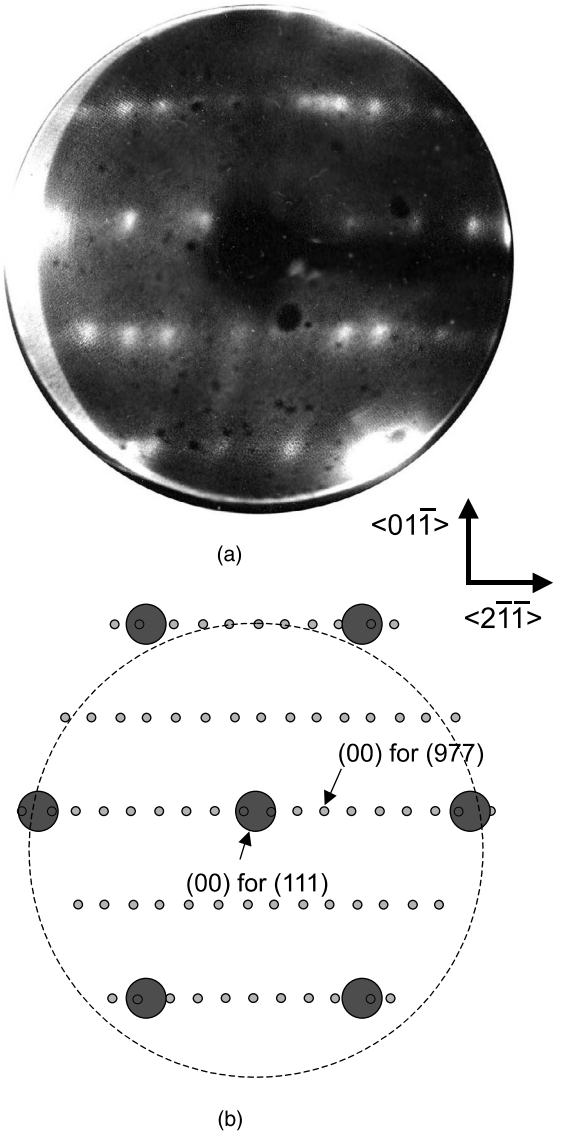

Fig. 5. (a) LEED pattern ($E_i = 51.3$ eV) of Ni[8(1 1 1) × (1 0 0)]–2(1d)-O step-edge localized overlayer. The step edges are aligned vertically with respect to the LEED screen. The two brightest spots on the edge of the screen are from the (1 1 1) terraces. The four rows of closely spaced spots arise from the oxygen overlayer. On the clean surface, diffraction from the steps is not visible except at the terrace spots. (b) Schematic representation of the LEED pattern in (a) showing the location of the specular spots for both surface normals. This drawing includes all of the possible spots for an ($n \times 2$) structure. Due to lack of coherence between steps for the step edge structure, destructive interference in the diffraction eliminates some of the spots as seen in (a). The dotted circle shows the area included in the LEED pattern in (a).

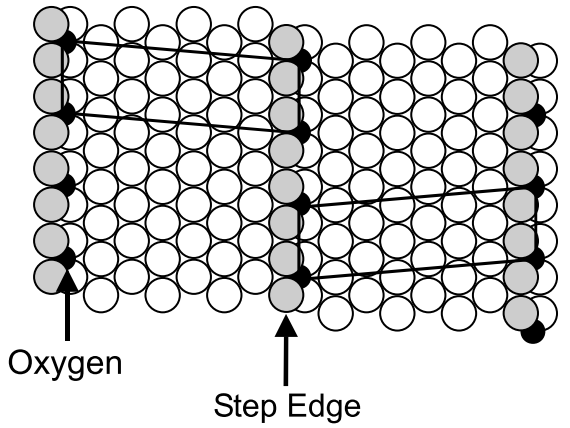

Fig. 6. Proposed structural schematic of the novel ($n \times 2$)-O phase, or Ni[8(1 1 1) × (1 0 0)]–2(1d)-O in microfacet notation, as derived from LEED data. Oxygen atoms occupy ever other four-fold hollow site in the (1 0 0) step troughs. Two different unit cells coexist due to the absence of imposed registry between oxygen rows adsorbed on neighboring step edges.

overlayer spots relative to the specular spot as a function of energy. The $p(2 \times 2)$ overlayer is a terrace-centered structure and it is evident that this overlayer converges on the terrace specular spot with increasing energy. The ($n \times 2$), however, is not terrace-centered but step-centered, i.e., its diffraction pattern is centered on the Ni(9 7 7) specular spot. This is corroborative evidence for an ($n \times 2$) step edge-stabilized structure. Fig. 6 illustrates the two unit cells that exist for oxygen adsorbed at the (1 0 0) step edges. Both geometries are possible since there is no imposed registry between oxygen rows on neighboring step edges. If there were oxygen atoms on the terraces, another unit cell would be expected to appear in the diffraction commensurate with the terrace specular spot; such terrace related spots were not detected.

In an attempt to further confirm the identification of the real space ($n \times 2$) unit cell, STM images of the surface were recorded at room temperature after forming the 2(1d)-O or ($n \times 2$) phase. Unfortunately, due to the corrugation associated with the step array and the nature of the local density of states for oxygen on metals, it was not possible to resolve the disordering and dissolution behavior of the oxygen with STM. (Bonding at step troughs makes the oxygen adatoms difficult to resolve by

STM imaging at room temperature.) However, the STM was used to eliminate other possible structures as discussed below, corroborating conclusions drawn from our LEED data. On other oxygen/stepped metal systems extensive facetting of the step array, which would be composed of step planes not parallel to the original steps, has been observed [37–39]. In another study, an ordered oxide facet that traverses multiple substrate step edges persists with a different normal than either the terraces or the original monatomic steps [40]. For our system, however, the STM images show that monatomic steps with the characteristic terrace width of clean Ni(9 7 7) dominate the surface as shown in Fig. 1.

3.2. Dissolution of oxygen: AES

Measurements were performed on the dissolution of 0.25 ML coverage of oxygen on the stepped nickel surface (Fig. 3a). Care was taken to avert the influence on LEED measurements of the strong interaction between high energy electrons (3 kV) used for AES and the chemisorbed oxygen. In order to avoid such electron damage to the oxygen overlayer, the oxygen (510 eV) and nickel (848 eV) Auger peak ratio for the oxygen exposure used to grow a $p(2 \times 2)$ overlayer was recorded as a function of temperature separately from observing the diffraction. Care was also taken to minimize the creation of oxide particles as a result of exposing the oxygen-covered nickel to a high energy electron beam. Stirniman et al. have shown that the oxidation rate for nickel can be significantly increased by swarms of secondary electrons created via doses of high energy electrons [41]. Since nickel oxide persists on the surface at higher temperatures than does chemisorbed oxygen, oxide particles created at a lower temperature would be able to contribute to the oxygen Auger peak intensity recorded at a subsequent higher temperature. Auger measurements were performed at each temperature on an unsampled region of the crystal to avoid the influence of oxide particles on oxygen concentration measurements. The crystal dwelled at each temperature for $\sim$5 min before Auger spectra were collected.

Compared to O/Ni(1 1 1), the Ni(9 7 7) system exhibits a more gradual oxygen dissolution curve (Fig. 3a) where significant loss of surface oxygen begins past 440 K. This temperature is considerably lower than 500 K, which was reported by Kortan and Park for oxygen on Ni(1 1 1) [32]. The temperature at which we observe the oxygen to fall below our detection limit, 565 K, is also lower than Kortan and Park's value. The onset temperature for oxygen dissolution into the selvedge or bulk regions of a crystal, however, is strongly determined by the history of oxidation for a particular sample. It is difficult to unequivocally determine the quantitative sensitivity of the dissolution process to various levels of embedded oxygen, but the effect on surface dissolution has been observed in many cases [34,42]. From the LEED data we know that diffraction persists up to this temperature. We propose that the dissolution curve presented in Fig. 3a contains two dissolution onsets, though only one is apparent. The initial stage, which dominates the adsorption behavior, is attributed to dissolution into the terraces at a temperature close to that observed for a Ni(1 1 1) surface and then, at a higher temperature, oxygen is lost from the step faces. The step edge bound oxygen may dissolve either through the step face or via detachment from the step followed by absorption into the terrace.

4. Discussion and conclusions

Introducing steps to this system has significantly altered the phase diagram of chemisorbed oxygen. It is not surprising that steps would have such an effect, as related results have been documented for hydrogen chemisorbed on nickel [36]. There are three noteworthy step-induced effects. First, unlike H/Ni(9 7 7), the transition temperature of the $p(2 \times 2)$-O phase is unaffected, but a coexisting Ni[8(1 1 1) $\times$ (1 0 0)]–2(1d)-O structure not observed on Ni(1 1 1) is anchored by the steps (Fig. 5).

The second major effect induced by the array of steps is the observation that the oxygen LEED spots become increasingly oblate with increasing temperature. Anisotropic diffraction of this nature suggests the existence of direction-dependent co-

herence lengths. We believe this to be evidence for ordered domains persisting locally in the vicinity of step edges above the terrace order–disorder transition temperature [43]. A similar effect was reported by van de Walle et al. [44] after they imaged the H/Ni(1 1 1) system with an STM and observed small domains of the (2×2)-2H structure at step edges persisting at room temperature despite disordering on the terraces at 270 K. Unfortunately, verifying this inhomogeneous disordering by analyzing the dimension-dependent coherence lengths for the adlayer is hindered by the steps themselves. There is streaking in the $\langle 2\bar{1}\bar{1} \rangle$ direction associated with the stepped surface; the spot widths in this direction involve a convolution of domain coherence length and step diffraction. Further studies with an STM would be most difficult given the high temperatures and binding sites involved, but low energy helium diffraction may have the potential to resolve this issue.

A third manifestation of step edge influence is a change in dissolution behavior. The generation of a step-registered structure after the 0.25 ML overlayer disorders and loses oxygen to dissolution suggests that there exist multiple dissolution stages. On Ni(1 1 1), oxygen will not dissolve below 500 K [32], but we observe a progressive dissolution into Ni(9 7 7) beginning even below 400 K (Fig. 5a). These temperatures, however, are strongly influenced by the oxidation history of the crystal in terms of oxygen population of selvedge and bulk regions of the material. We believe that oxygen dissolves anisotropically: it dissolves into the terraces and remains near the step edges at higher temperatures. We propose a kinetic difference in dissolution of oxygen between terrace (1 1 1) and step (1 0 0) crystallographies resulting from the difference in bonding between four-fold and three-fold hollow sites found on the step and terrace faces of this surface, respectively. The O–Ni bond strength derived from heat of adsorption measurements is 5.39 eV for the (1 0 0) face and 4.87 eV for (1 1 1) [45]. Assuming a similar barrier height for dissolution, this difference produces a higher effective kinetic barrier for absorption via the steps. It is difficult to unequivocally determine the dissolution pathway for oxygen bound at the steps, but it is clear that the presence of steps enables oxygen to remain on the surface at higher temperatures. A Ni vicinal surface with identical geometry on the steps and terraces would not exhibit such two-step oxygen dissolution behavior.

5. Summary

We have studied the interaction between ordered overlayers of oxygen and a stepped Ni(9 7 7) surface in order to isolate the effect of a regular array of steps on the adsorbate phase diagram. Our results demonstrate that introducing steps produces three significant effects, namely: (i) adding a previously unknown step-stabilized and anchored ordered oxygen phase, Ni[$8(1\,1\,1) \times (1\,0\,0)$]–2(1d)-O, that is stable at much higher temperatures than ordered phases on the flat surface; (ii) promoting spatially inhomogeneous disordering where oxygen disorders in the center of the terraces before doing so in the proximity of the step edges; and (iii) introducing multiple stages for oxygen dissolution into the bulk. All of these effects are intimately related to the step-doubling and resingling reconstructions that occur on this stepped surface as a function of temperature and oxygen coverage [15,16]. The stabilizing influence of the steps on adsorbate overlayers provides a direct competition in the free energy balance that governs other step phenomena such as step edge mobility and step reconstructions leading to facetting.

Acknowledgements

We gratefully acknowledge Lyle Roelofs for useful discussions about this system. This work was supported by the Air Force Office of Scientific Research and, in part, by the NSF-MRSEC at the University of Chicago, award no DMR-9808595.

References

[1] M.J. Stirniman, W. Li, S.J. Sibener, J. Vac. Sci. Technol. A 13 (1995) 1574.
[2] W. Li, M.J. Stirniman, S.J. Sibener, Surf. Sci. 329 (1995) L593.

[3] B.D. Zion, A.T. Hanbicki, S.J. Sibener, Surf. Sci. 417 (1998) L1154.
[4] S.A. Raspopov, A.G. Gusakov, A.G. Voropayev, A.A. Vecher, B.K. Grishin, J. Alloys Compounds 227 (1995) 5.
[5] W.-D. Wang, N.J. Wu, P.A. Thiel, J. Chem. Phys. 92 (1990) 2025.
[6] P.H. Holloway, J.B. Hudson, Surf. Sci. 43 (1974) 123.
[7] P.H. Holloway, J.B. Hudson, Surf. Sci. 43 (1974) 141.
[8] P.H. Holloway, J. Vac. Sci. Technol. 18 (1981) 653.
[9] A. Atkinson, D.W. Smart, J. Electrochem. Soc. 135 (1988) 2886.
[10] O.L. Warren, P.A. Thiel, J. Chem. Phys. 100 (1994) 659.
[11] C.R. Brundle, J.Q. Broughton, in: A. King, D.P. Woodruff (Eds.), The Chemical Physics of Solid Surfaces and Heterogeneous Catalysis, vol. 3, part A, Elsevier, Amsterdam, 1990, p. 132.
[12] I.L. Bolotin, A. Kutana, B. Makarenko, J.W. Rabalais, Surf. Sci. 472 (2001) 205.
[13] S. Hildebrandt, C. Hagendorf, T. Doege, C. Jeckstiess, R. Kulla, T. Uttich, J. Vac. Sci. Technol. A 18 (2000) 1010.
[14] G. Tisdale, S.J. Sibener, Surf. Sci. 311 (1994) 360.
[15] T.P. Pearl, S.J. Sibener, J. Chem. Phys. 115 (2001) 1916.
[16] L. Niu, D.D. Koleske, D.J. Gaspar, S.F. King, S.J. Sibener, Surf. Sci. 356 (1996) 144.
[17] E. Schmidtke, C. Schwennicke, H. Pfnür, Surf. Sci. 312 (1994) 301.
[18] R. Koch, O. Haase, M. Borbonus, K.H. Rieder, Surf. Sci. 272 (1992) 17.
[19] L. Eierdal, F. Besenbacher, E. Laegsgaard, I. Stensgaard, Surf. Sci. 312 (1994) 31.
[20] L.D. Roelofs, A.R. Kortan, T.L. Einstein, R.L. Park, Phys. Rev. Lett. 42 (1981) 1465.
[21] Z. Li, X. Liang, M.L. Stutzman, J.A. Spizuoco, S. Chandavarkar, R.D. Diehl, Surf. Sci. 327 (1994) 121.
[22] T. Zambelli, J. Wintterlin, J. Trost, G. Ertl, Science 273 (1996) 1688.
[23] S.H. Payne, H.J. Kreuzer, Surf. Sci. 399 (1998) 135.
[24] J.H. Ferris, J.G. Kushmerick, J.A. Johnson, P.S. Weiss, Surf. Sci. 446 (2000) 112.
[25] M.M. Kamna, S.J. Stranick, P.S. Weiss, Science 274 (1996) 118.
[26] L. Niu, D.J. Gaspar, S.J. Sibener, Science 268 (1995) 847.
[27] T.P. Pearl, S.J. Sibener, Rev. Sci. Instrum. 71 (2000) 124.
[28] S. Mroz, Surf. Sci. 51 (1975) 365.
[29] G. Witte, J. Braun, D. Nowack, L. Bartels, B. Neu, G. Meyer, Phys. Rev. B 58 (1998) 13224.
[30] B. Lang, R.W. Joyner, G.A. Somorjai, Surf. Sci. 30 (1972) 454.
[31] H.E. Dorsett, E.P. Go, J.E. Reutt-Robey, N.C. Bartelt, Surf. Sci. 342 (1995) 261.
[32] A.R. Kortan, R.L. Park, Phys. Rev. B 23 (1981) 6340.
[33] C. Schwennicke, H. Pfnür, Phys. Rev. B 56 (1997) 10558.
[34] P.A. Holloway, R.A. Outlaw, Surf. Sci. 111 (1981) 300.
[35] M. Sokolowski, H. Pfnür, Phys. Rev. Lett. 63 (1989) 183.
[36] A.T. Hanbicki, S.B. Darling, D.J. Gaspar, S.J. Sibener, J. Chem. Phys. 111 (1999) 9053.
[37] E. Hahn, H. Schief, V. Marsico, A. Fricke, K. Kern, Phys. Rev. Lett. 72 (1994) 3378.
[38] P.J. Knight, S.M. Driver, D.P. Woodruff, Surf. Sci. 376 (1997) 374.
[39] D.A. Walko, I.K. Robinson, Phys. Rev. B 59 (1999) 15446.
[40] M. Bäumer, D. Cappus, H. Kuhlenbeck, H.J. Freund, G. Wilhelmi, A. Brodde, H. Neddermeyer, Surf. Sci. 253 (1991) 116.
[41] M.J. Stirniman, W. Li, S.J. Sibener, J. Chem. Phys. 103 (1995) 451.
[42] T.P. Pearl, S.B. Darling, L. Niu, D.D. Koleske, D.J. Gaspar, S.F. King, S.J. Sibener, in preparation.
[43] L. Roelofs, personal communication.
[44] G.F.A. van de Walle, H. Van Kempen, P. Wyder, C.J. Flipse, Surf. Sci. 181 (1987) 27.
[45] J.T. Stuckless, C.E. Wartnaby, N. Al-Sarraf, S.J.B. Dixon-Warren, M. Kovar, D.A. King, J. Chem. Phys. 106 (1997) 2012.